Lab on a Chip

ARTICLE

Received 00th January 20xx,
Accepted 00th January 20xx

DOI: 10.1039/x0xx00000x

www.rsc.org/

On-chip polyelectrolyte coating onto magnetic droplets – Towards continuous flow assembly of drug delivery capsules

Ali Q. Alorabi,‡[a] Mark D. Tarn,§[a] Jenifer Gómez-Pastora,[b] Eugenio Bringas,[b] Inmaculada Ortiz,[b] Vesselin N. Paunov[a] and Nicole Pamme*[a]

Polyelectrolyte (PE) microcapsules for drug delivery are typically fabricated via layer-by-layer (LbL) deposition of PE layers of alternating charge on sacrificial template microparticles, which usually requires multiple incubation and washing steps that render the process repetitive and time-consuming. Here, ferrofluid droplets were explored for this purpose as an elegant alternative of templates that can be easily manipulated via an external magnetic field, and require only a simple microfluidic chip design and setup. Glass microfluidic devices featuring T-junctions or flow focusing junctions for the generation of oil-based ferrofluid droplets in an aqueous continuous phase were investigated. Droplet size was controlled by the microfluidic channel dimensions as well as the flow rates of the ferrofluid and aqueous phases. The generated droplets were stabilised by a surface active polymer, polyvinylpyrrolidone (PVP), and then guided into a chamber featuring alternating, co-laminar PE solutions and wash streams, and deflected across them by means of an external permanent magnet. The extent of droplet deflection was tailored by the flow rates, the concentration of magnetic nanoparticles in the droplets, and the magnetic field strength. PVP-coated ferrofluid droplets were deflected through solutions of polyelectrolyte and washing streams using several iterations of multilaminar flow designs. This culminated in an innovative "Snakes-and-Ladders" inspired microfluidic chip design that overcame various issues of the previous iterations for the deposition of layers of anionic poly(sodium-4-styrene sulfonate) (PSS) and cationic poly(fluorescein isothiocyanate allylamine hydrochloride) (PAH-FITC) onto the droplets. The presented method demonstrates a simple and rapid process for PE layer deposition in <30 seconds, and opens the way towards rapid layer-by-layer assembly of PE microcapsules for drug delivery applications.

Introduction

Polymer multilayer capsules (PMLCs) have attracted a great deal of attention in areas as wide ranging as drug delivery,[1-3] biosensors[4, 5] and bioreactors.[6, 7] Conventionally, these microcapsules are fabricated using a layer-by-layer (LbL) technique (Fig. 1a),[8, 9] involving the deposition of around ten layers of oppositely charged polyelectrolytes (PEs) onto a sacrificial template species, such as colloidal particles and inorganic crystals,[10] biological cells,[11, 12] or droplets.[13, 14] The template is then dissolved to leave a hollow capsule, which can be further loaded with active components. The incorporation of stimuli-responsive moieties into the PE layers allows the PMLCs to swell or contract upon exposure to various stimuli, including pH, light, magnetism, salt, and glucose.[15] Exploitation of this feature provides a powerful strategy for development of drug delivery vehicles by which drugs can be encapsulated and then released upon exposure to a specific trigger. However, the LbL method of manufacturing PMLCs is time-consuming and labour intensive, requires multiple PE deposition and washing steps that are typically performed via centrifugation,[16, 17] magnetic separation or membrane filtration[18] of the templates.

The combination of microfluidic devices[19] and multilayered PEs has shown some promise to speed up this technology for a number of applications.[20]

[a] School of Mathematics and Physical Sciences, University of Hull, Cottingham Road, Hull, HU6 7RX, UK. E-mail: n.pamme@hull.ac.uk; Tel: +44 (0) 1482 465027; Fax: +44 (0) 1482 466410.
[b] Department of Chemical and Biomolecular Engineering, University of Cantabria, Av. de los Castros s/n, 39005 Santander, Cantabria, Spain.

‡ Current address: Albaha University, Prince Mohammad Bin Saud, Al Bahah 65527, Saudi Arabia.
§ Current address: School of Earth and Environment, University of Leeds, Woodhouse Lane, Leeds, LS2 9JT, UK.

† Electronic Supplementary Information (ESI) available: Further details on the various shallow and deep chip designs tested, and the optimisation of droplet generation and deflection for the shallow, deep, and "Snakes-and-Ladders" chip designs. Videos are also provided of droplet deflection in the shallow chip design (ESI Video 1), droplet generation in the deep chip design DGF4 (ESI Video 2), droplet deflection in the deep chip design (ESI Video 3), and droplet deflection in the "Snakes-and-Ladders" chip design (ESI Video 4). See DOI: 10.1039/x0xx00000x

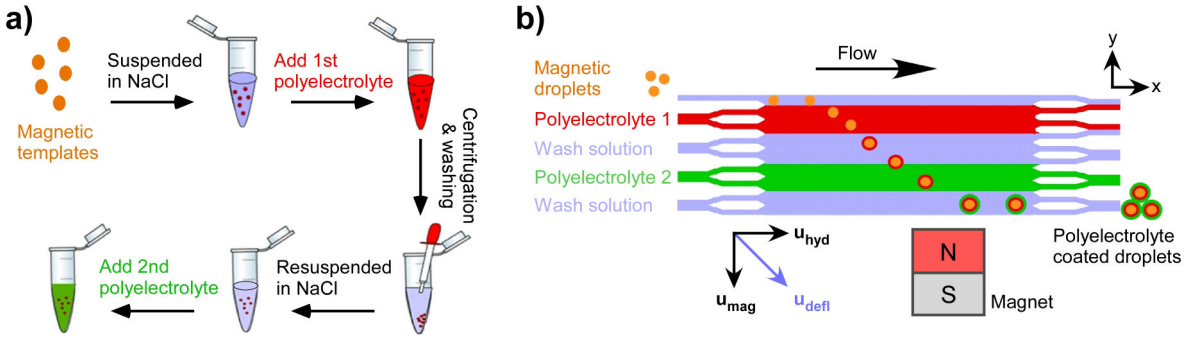

Fig. 1 (a) Conventional layer-by-layer (LbL) deposition of polyelectrolytes (PE) onto magnetic templates for the fabrication of PE multi-layered capsules (PMLCs). Multiple washing steps are required after the deposition of each PE layer, yielding a time-consuming and laborious procedure. (b) The concept of continuous flow LbL deposition of PEs via the deflection of magnetic templates (e.g. droplets) through multi-laminar flow streams of PE and washing solutions enables rapid PE deposition.

In particular, microfluidic technology offers an attractive alternative for LbL fabrication of PMLCs due to the potential for continuous flow processing in a rapid and automated manner,[21] with a particular view to the fabrication of drug delivery vehicles.[22] For example, Kaufman et al.[23] employed water-soluble and oil-soluble PEs to form PE bilayers on water-in-oil droplets during their generation, later expanding the technique to form nanoparticle-PE/protein-PE complexes on the droplets.[24] Zhang et al.[25] employed a similar technique using an aqueous two-phase system rather than immiscible fluids. However, while this one-step process is simple and fast for PE bilayer formation, the addition of more layers to form a full PMLC would be non-trivial due to the cumbersome construction of the capillary-in-capillary microfluidic devices.

Multilaminar flow processing[26] in microfluidic devices offers several advantages for the production of PMLCs. Here, multiple laminar flow streams are generated containing parallel, alternating reagent and washing solutions, through which the core templates (particles, cells or droplets) are passed consecutively in order to perform various procedures. Complex channels or micro-pillar designs have been employed for manipulating the templates in flow for PE deposition. For example, Priest et al.[27] employed a channel with multiple side channels to sequentially exchange the liquid environment around droplets for the deposition of up to three layers of polymer. Kantak et al.[28] used an array of micropillars to shuttle droplets back-and-forth across three laminar flows of PEs and washing solution, in a form of microfluidic "pinball", building up to three bilayers onto the oil droplet template. Ayan *et al.*[29] employed an acoustofluidic approach that used tilted-angle standing surface acoustic waves (taSSAWs) to deflect particles and cells through streams of PE to form a bilayer coating. However, while these methods offer manipulation of the templates based on their intrinsic properties, each requires complicated channel designs or fabrication that require tuning for the specific templates.

Arguably, the most popular method for manipulating particles, cells and droplets through multilaminar flow streams is via the use of magnetic forces, largely due to the ease with which such forces can be employed in microfluidic devices,[30-33] including the coating of magnetic particles fluids in an immiscible phase.[34-36] Previously, we demonstrated a method in which magnetic particles were deflected through multiple reagent and washing streams via magnetic forces for immunoassays[37-41] and DNA hybridisation,[39, 42] and applied it to the deposition of a single layer of PE onto magnetically coated yeast cells.[43] However, we found that the cationic PE-coated magnetic cells were susceptible to electrostatic adhesion to the microchannel surface. Here, we explore a different form of template for PMLC fabrication in order to overcome the adhesion issues previously reported.

Ferrofluids are colloidal suspensions iron oxide nanoparticles (5 - 20 nm in diameter) dispersed in a carrier fluid that can be aqueous or oil-based and stabilised via a surfactant or polymer coating.[44] The size of the particles ensures that the ferrofluid is superparamagnetic: the fluid is attracted towards a magnetic field, but when the field is removed the nanoparticles lose their magnetisation and are able to disperse freely in the suspension. The ability to manipulate the magnetic fluid by an external magnetic field has seen its use for a number of applications in microfluidics, including pumping, valving, and the deflection of microparticles and cells.[44-46] Since ferrofluids can be oil-based or aqueous, they can be used to generate magnetic droplets as easily as any other oil/water combination[47-50] by using a continuous phase that is immiscible with the ferrofluid,[51-62] while non-magnetic droplets have also been formed in a ferrofluid continuous phase.[63, 64]

Our research team,[53] and other authors,[54, 62] have previously demonstrated that magnetic droplets can be easily and effectively deflected across a microfluidic chamber via an external magnetic field, in a similar fashion to the deflection of magnetic microparticles and cells in multilaminar flow processes. Here, we employ an oil-based ferrofluid for the generation of magnetic droplets as PMLC templates and their deflection across multilaminar flow streams of PE solutions (Fig. 1b) towards the rapid and automated fabrication of PMLCs. The layer of immiscible fluid between the droplets and the channel walls as well as the droplet PE coating were expected to reduce the extent to which the magnetic

templates stick to the channel surface, thus overcoming some of the previous challenges encountered.

We further show the various iterations of the microfluidic devices and techniques we employed in order to demonstrate how a number of different issues, which could be experienced by researchers developing similar systems, were addressed. These iterations include: (i) a shallow chip design, (ii) a "deep" chip design, and (iii) a chip design inspired by the "Snakes-and-Ladders" boardgame that represented a culmination of various improvements based on experiences and problems with the previous shallow and deep designs. All three designs are described here to illustrate the various issues encountered and to help other researchers avoid some possible problems, while the main focus is on the final "Snakes-and-Ladders" design.

Theory of magnetic deflection

The trajectory of magnetic objects in a chamber ($\mathbf{u_{defl}}$), for the configuration shown in Fig. 1b, depends on the velocity vector of the applied flow rate ($\mathbf{u_{hyd}}$) in the x-direction and the magnetically-induced velocity of the object towards the magnet ($\mathbf{u_{mag}}$), largely acting in the y-direction, as given by

$$\mathbf{u_{defl}} = \mathbf{u_{hyd}} + \mathbf{u_{mag}} \quad (1)$$

In the absence of a magnetic field, magnetic objects, in this case ferrofluid droplets, would follow the hydrodynamic flow in the *x*-direction and leave the chamber via the exit channel directly opposite the inlet. However, in the presence of a magnetic field, a magnetic force ($\mathbf{F_{mag}}$) acts on the magnetic droplets and pulls them in the *y*-direction, as shown in Fig. 1b. The trajectory that the magnetic droplets follow across the chamber[53, 54, 65] depends on the extent of $\mathbf{F_{mag}}$:[30, 53]

$$\mathbf{F_{mag}} = \frac{\Delta\chi\, N\, V_m\, (\mathbf{B}\cdot\nabla)\mathbf{B}}{\mu_0}. \quad (2)$$

Here μ_0 is the permeability of free space ($4\pi x10^{-7}$ H m^{-1}), $\Delta\chi$ is the difference in magnetic susceptibility (χ_p - χ_m) between a magnetic droplet (χ_p) and surrounding medium (χ_m), *N* is the number of magnetic nanoparticles within a droplet, V_m is the volume of a magnetic nanoparticle, **B** is the magnetic flux density, and $\nabla\mathbf{B}$ is the gradient of the magnetic flux density. Typical values of $(\mathbf{B}\cdot\nabla)\mathbf{B}$ generated by NdFeB magnets across a microfluidic chamber are on order of 10 - 100 mT mm^{-1}.[66, 67] When a magnetic droplet moves with a constant velocity through a medium due to a magnetic force, the latter is opposed by an equal force caused by the viscous drag, $\mathbf{F_{vis}}$:

$$\mathbf{F_{vis}} = \mathbf{F_{mag}}. \quad (3)$$

The viscous drag force, $\mathbf{F_{vis}}$, in turn, is a function of the droplet radius, *r*, the viscosity of the surrounding medium, η, and the velocity of the droplet due to the magnetic field, $\mathbf{u_{mag}}$, as per Stokes' law:

$$\mathbf{F_{vis}} = 6\,\pi\,\eta\,r\,\mathbf{u_{mag}}. \quad (4)$$

Equations (2), (3) and (4) can thus be combined and rearranged to give the extent of $\mathbf{u_{mag}}$ of the droplet in the *y*-direction while it is deflected across a reaction chamber, in terms of the $\mathbf{F_{mag}}$ and the viscous drag:

$$\mathbf{u_{mag}} = \frac{\mathbf{F_{mag}}}{6\,\pi\,\eta\,r}. \quad (5)$$

Equation (5) describes how the magnetic force on the droplet affects its deflection ($\mathbf{u_{defl}}$) across the reaction chamber, as per equation (1).

Experimental

Chemicals

Oil-based ferrofluid (FF, EMG901), containing a suspension of 10 nm diameter magnetic nanoparticles at a concentration of 11.8 vol% was purchased from Ferrotec (USA). Sodium dodecyl sulfate (SDS), poly(vinylpyrrolidone) (PVP, M_w = 40 kDa), Tween20, Tween60, poly(sodium-4-styrene sulfonate) (PSS, M_w ≈ 70 kDa), poly(fluorescein isothiocyanate allylamine hydrochloride) (PAH-FITC, M_w ≈ 15 kDa), poly(acrylic acid) (PAA, M_w ≈ 250 kDa), Rhodamine 123 (Rhod123), 1-ethyl-3-(3-dimethylaminopropyl) carbodiimide hydrochloride (EDC), *N*-hydroxysuccinimide (NHS), and sodium acetate trihydrate were purchased from Sigma Aldrich (Dorset, UK). Cyclohexane, dichloromethane (DCM), N,N-dimethylformamide (DMF), and acetic acid were obtained from Fisher Scientific (Loughborough, UK). Blue and red inks (Printer Refill Ink, catalogue number: 207-9106) were brought from a local Tesco supermarket.

Preparation of Rhodamine 123-tagged poly(acrylic acid)

The weak anionic polyelectrolyte, poly(acrylic acid) (PAA), fluorescently labeled with Rhodamine 123 (Rhod123) using the method described by Laguecir et al.[68] Solutions of 50 mM EDC and 100 mM NHS were prepared in 10 mL of water, then 1.5 g of PAA immediately added and mixed with the EDC/NHS solution, before being adjusted to pH 5.5. A 1 % w/v solution of Rhodamine 123 was prepared in 2 mL DMF and added to the EDC/NHS/PAA mixture, then left in the dark overnight under agitation. The mixture was then dried completely in a freeze drier and re-suspended in water at pH 9, followed by five extractions with DCM. The free Rhodamine 123 was dialysed three times using a dialysis tube (Spectra/Por 1 Dialysis membrane, 6-8 kD MWCO, Spectrum Laboratories, The Netherlands) for at least 8 h, each time with sterile deionised water (once at pH 3 and twice at pH 5.5).

Microfluidic chip designs and fabrication

Three types of microfluidic devices were employed for the generation of droplets and their deflection through reagent and washing streams (Fig. 2): (i) a **shallow chip** design, (ii) a **deep chip** design, and (iii) a **"Snakes-and-Ladders" chip** design.

Droplets were generated using either flow focusing (DGF) or T-junction (DGT) designs. Chips were fabricated in glass (1 mm thick plates, B270 glass, Telic, CA, USA) using conventional photolithography and wet etching techniques.[69] Access holes (400 μm diameter) were drilled, and the glass plates thermally bonded together. The chips were placed in an aluminium chip holder (Fig. 2b) for performing the experiments.

Shallow chip designs. These chips were composed of a single etched plate, containing both the droplet generation and reaction chamber design, etched to a depth of 20 μm and bonded to an unetched glass plate. (Fig. 2a and ESI Fig. S1) featured a flow focusing junction (designated DGF1; Fig. 2a and ESI Fig. S1) or a T-junction (DGT2 and DGT3, shown in ESI Figs. S2b and S2c, respectively) for droplet generation, with DGF1 being selected for use in experiments following initial tests (further details on DGT2 and DGT3 are given in ESI Section 1). The DGF1 design had a 50 μm wide inlet for the oil-based ferrofluid dispersed phase (DP, inlet 1) and a 100 μm wide inlet for the continuous aqueous phase (CP, inlet 2), while the nozzle was 50 μm wide. This fed into an 8 mm long by 2.7 mm wide (before etching) reaction chamber, with branched inlet channels (inlets 3-6, 120 μm wide each) and five outlet channels (120 μm wide each). The design was etched into a single glass plate to a depth of 20 μm, access holes drilled into the same plate, and it was bonded to an unetched glass plate.

Deep chip designs. These chips consisted of two etched glass plates that were bonded together. The top plate featured a droplet generation region that consisted of either a flow focusing junction (DGF4, see Fig. 2c) or a T-junction (DGT5 or DGT6, see ESI Fig. S6), and were interchangeable with a bottom plate design that comprised a reaction chamber (see Fig. 2d and ESI Fig. S6). The droplet generation top plate was etched to a depth of 20 μm, while the bottom plate with the reaction chamber was etched to a depth of 100 μm. Droplet generation design DGF4 was selected for use following initial tests of all three designs. DGF4 contained a flow focusing junction with one inlet (140 μm wide after etching) for the aqueous continuous phase (CP) and one inlet (90 μm wide) for the oil-based ferrofluid dispersed phase (DP), while the nozzle was 50 μm wide. Designs DGT5 and DTG6 are described in detail in ESI Section 2.1.

The reaction chamber in the bottom plate was 8.2 mm long and 4.3 mm wide after etching, with inlets 3-6 leading into the chamber for the generation of multi-laminar flow streams, and five outlets (Fig. 2d and ESI Figs. S6d-f). The inlet and outlet channels were each 225 μm wide following the etching process. The top and bottom etched plates were carefully aligned, such that the droplet generation channel of the top layer fed into the droplet inlet of the chamber in the bottom layer, before being thermally bonded together (Fig. 2d and ESI Figs. S6d,e). Further details on the deep chip design are provided in Section 2 of the ESI.

"Snakes-and-Ladders" chip design. This was based on similar principles to the deep chip design, in that it was prepared from a droplet generation top plate (etched to a depth of 20 μm) that were interchangeable with a bottom plate containing channels for droplet processing (etched to a depth of 100 μm). Rather than the reaction chamber of the previous examples, the bottom layer instead featured a series of five parallel channels (400 μm width each after etching) that were interconnected by diagonal channels (each 250 μm wide after etching) in order to allow the droplets to pass between channels at specific junctions, reminiscent of the "Snakes-and-Ladders" board game (Fig. 2e). As before, the two etched plates were aligned and bonded such that the droplets fed from the droplet generation structure in the top layer into the parallel channels in the bottom layer (Fig. 2f).

Microfluidic chip setup

The chips were mounted into the aforementioned aluminium chip holder that was designed and fabricated in-house (Fig. 2b) based on those described by Phurimsak *et al*.[40] NanoPort ferrules (Presearch, UK) and TinyTight PEEK nuts (Presearch, UK) that were screwed into the chip holder enabled a tight seal between the access holes of the glass chip and fused silica capillaries (150 μm i.d., 375 μm o.d., CM Scientific, UK). The capillaries connected to the inlet holes of the chip were connected to 500 μL glass syringes (SGE, Sigma-Aldrich, UK) that were driven by three precision syringe pumps (PHD2000, Harvard Apparatus, Biochrom, UK): one pump for the DP and one pump for the CP for droplet generation, with one pump for the multiple reagent and washing solutions used for processing of the droplets.

Lab on a Chip

ARTICLE

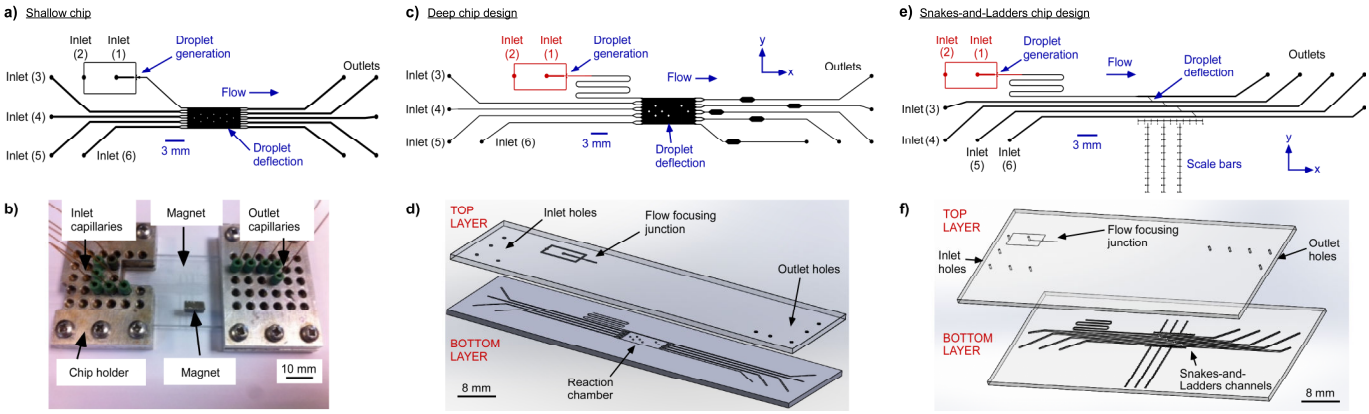

Fig. 2 Different generations of chip designs and setup for performing droplet generation and PE deposition in continuous flow. (a) Shallow chip design (designated DGF4) featuring a flow-focusing droplet generation junction and a chamber for the deflection of droplets through multilaminar flow streams. The design was etched to a depth of 20 µm. (b) Aluminium chip holder used to interface each of the glass chips to inlet and outlet capillaries. A magnet was placed atop the chip, below the reaction chamber. (c-f) Chip designs and exploded schematics of glass chips composed of two etched plates: a top layer featuring an interchangeable droplet generation junction (20 µm deep, shown in red in the CAD designs), and a bottom layer featuring a channel structure for the magnetic deflection of droplets through reagent and washing streams (100 µm deep). (c) CAD drawing of the "deep" chip design with a single reaction chamber for the generation of multi-laminar flow streams, and (d) an exploded view of the two-part deep chip. (e) CAD drawing of the "Snakes-and-Ladders" chip design featuring five interconnected parallel channels, and (f) an exploded view of the two-part chip.

Droplet generation and deflection was observed via an inverted fluorescence microscope (Eclipse Ti, Nikon, UK) equipped with a high resolution CCD camera (Retiga EXL, Media Cybernetics, UK) or a colour CCD camera (MTV-63V1N, Mintron, Taiwan). ImageJ freeware (https://imagej.nih.gov/ij/) was used for the analysis of droplet size and fluorescence intensity. Magnetic fields were generated by external magnets (Magnet Sales, UK), made from neodymium-iron-boron (NdFeB) or sintered samarium cobalt (SmCo), that were placed onto the glass chips and precisely positioned near the lower edge (in the y-direction) of either the reaction chamber, for shallow and deep chips or the parallel channel 5 of the "Snakes-and-Ladders" chip. Positioning of the magnets was aided by the incorporation of scale bars into the chip designs (see Fig. 2f for example; the scale bars are not shown in all of the images here but were present in each of the fabricated devices).

On-chip droplet generation studies

The generation of droplets was tested using each of the three chip designs, and in the flow focusing and T-junction versions of each. Only the flow focusing versions (designated DGF) are discussed here, while the T-junction designs (designated DGT) are described in the ESI. In all cases, the oil-based ferrofluid dispersed phase (DP) was pumped into inlet 1 at 1 to 10 µL h^{-1}, while the aqueous continuous phase (CP) was pumped into inlet 2 at flow rates that varied from 50 to 500 µL h^{-1}, depending on the experiment, in order to study the effect on magnetic droplet size. The CP contained either SDS solution (1 % w/v) when using the shallow chip design or PVP solution (10 mg mL^{-1}) when using the deep or "Snakes-and-Ladders" chip design.

When using the shallow chip design, an aqueous solution of Tween20 (0.5 % v/v) was pumped into inlets 3-6 at flow rates between 100 and 500 µL h^{-1}. On the other hand. when using the deep or "Snakes-and-Ladders" chip designs, sodium acetate buffer (20 mM, pH 4) containing 0.05 % v/v Tween20 solution was pumped into inlets 3-6 at flow rates ranging from 100 to 1000 µL h^{-1}. Specific details of flow rates used are provided in the ESI.

On-chip droplet deflection studies

The magnetic deflection of the droplets across the chambers/channels was studied by varying the flow rates in the chamber and by varying the magnet type, size, and distance from the chamber. The aqueous solutions pumped into the chambers or parallel channels (i.e in inlets 3-6), depending on the chip design, and their flow rates were as described in the previous section, and only the flow focusing droplet generation designs (DGF) were used. In all cases, the magnet was placed on top of the glass chip, near to the lower edge (in the y-direction) of the chamber.

A cylindrical 15 mm Ø x 5 mm NdFeB magnet was used for the shallow chip design tests. Three types of rectangular magnets were tested with the deep chip design: a 2 x 2 x 5

mm^3 NdFeB magnet, a 3 x 3 x 5 mm^3 NdFeB magnet, or a 3 x 4.8 x 7.3 mm^3 SmCo, and they were placed at varying distances (from 1.5 mm to 10.5 mm) from the chamber/channel. The same SmCo magnet was employed for the "Snakes-and-Ladders" chip design. Further specific details for each test are provided in the ESI.

In the case of the tests performed using the deep chip designs, simulations of the magnetic flux density (**B**) across the reaction chamber were generated for each combination of magnet size and distance from the chamber using Finite Element Method Magnetics software (FEMM 4.2, www.femm.info) (ESI Figs. S8-S9). Similarly, in the case of the "Snakes-and-Ladders" chip design, a computational analysis of the magnetic flux density and magnetic force ($\mathbf{F_{mag}}$) across the channels was performed as described by Gómez-Pastora et al. [70, 71] Furlani's analytical model[72] was employed for calculating the magnetic field and gradient, while the force on the droplets was obtained after estimating the magnetic content of each droplet. These equations were resolved using MatLab v.2015 software (The MathWorks, Inc.).

On-chip droplet deflection through multilaminar streams

Following the magnetic deflection tests, the ability to deflect droplets through multilaminar flow streams was investigated. For each chip design, alternating streams of red and blue inks were generated across the chamber (for the shallow or deep chips) or parallel channels (for the "Snakes-and-Ladders" chips) by pumping the inks into inlets 3-6 at flow rates of 100 μL h^{-1} each for the shallow chips, 200 μL h^{-1} for the deep chip, and 300 μL h^{-1} each for the "Snakes-and-Ladders" chips. Deflection was achieved using the magnet types, sizes and distances determined from the previous tests for each type of chip design. Likewise, the flow rates and solutions used for droplet generation were based on the previous droplet generation results.

Finally, multilaminar flow streams of PEs and washing solutions were generated across the chambers/parallel channels in order to perform PE deposition on the droplets. The same flow rates were used for each chip as for the ink tests. For the shallow chips, fluorescently labelled and cationic PAH-FITC (1 mg mL^{-1}) was pumped into inlet 5, while washing solutions of Tween20 (0.5 % v/v) were pumped into inlets 3, 4, and 6. In the case of the deep chips, a stream of fluorescently labelled and anionic PAA-Rhod123 was pumped into inlet 4 while Tween20 (0.05 % v/v) solution was introduced into inlets 3, 5, and 6. Finally, for the "Snakes-and-Ladders" chips, negatively charged PSS (10 mg mL^{-1}) was pumped into inlet 4 while fluorescently labelled and cationic PAH-FITC (1 mg mL^{-1} with 0.05 % v/v Tween60) was pumped into inlet 6, and purified water was used as the washing solution via inlets 3 and 5.

Results and discussion

The shallow, deep, and "Snakes-and-Ladders" chip designs were developed as iterations on each other as various issues were encountered and addressed. The following sections describe the development of these iterations to with a view to helping other researchers avoid some of those issues, and to demonstrate how solving those issues culminated in the final "Snakes-and-Ladders" device.

Magnetic droplet manipulation in the shallow chip design

In the first multilaminar flow design, magnetic droplets were formed and deflected in a 20 μm deep channel structure, providing an initial platform to determine the viability of PE deposition on magnetic droplets in continuous flow. Thus, this required that a number of principles of the concept be verified, including the generation of magnetic droplets, their controlled deflection through the reaction chamber via a magnetic field, their deflection through multilaminar flow streams, and finally their deflection through a PE stream for deposition of the PE onto the droplets. Firstly, the ability to form and manipulate magnetic droplets was investigated using the flow focusing and T-junction chip designs. Magnetic droplets were prepared from a DP of oil-based ferrofluid and an aqueous CP of SDS (1 % w/v).

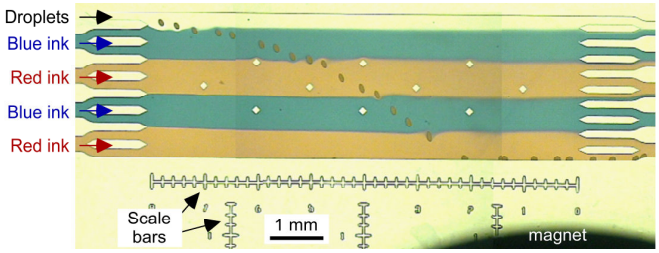

Fig. 3 Photograph showing the deflection of ferrofluid droplets across the reaction chamber towards an external NdFeB magnet using a shallow chip design (DGF1). Red and blue ink streams were generated to visualise the flow streams and demonstrate the minimal diffusion between them, as well as the minimal disturbance caused by the magnetic droplets as they passed from one ink stream to another.

Using the flow focusing DGF1 design, the droplet diameter could be controlled between 69.9 ± 6.1 μm and 137.4 ± 10.1 μm (in the microchannel) by varying the CP flow rate between 50 and 500 μL h^{-1} while keeping the DP flow rate constant at 2 μL h^{-1} (ESI Fig. S2). Details of the T-junction-based droplet generation tests are also shown ESI Fig. S3.

Droplets were then generated and deflected across the width (in the *y*-direction) of the reaction chamber in the DGF1 chip via a 15 mm Ø x 5 mm NdFeB magnet, and the flow rates were varied in order to achieve an optimal path across the reaction chamber, such that they exited the chip via outlet 5 (ESI Fig. S4 and Table S1). In order to then test the ability to deflect the magnetic droplets through multilaminar flow streams, alternating streams of red and blue inks were generated across the chamber and the magnetic droplets were successfully deflected consecutively through each stream, as shown in Fig. 3. Negligible crossover of inks was observed as the droplets passed from one ink stream to the next. The deflection of magnetic droplets through the ink streams can be

observed in "**ESI Video 1 - Droplet deflection in shallow chip design.mp4**".

Finally, in order to perform multilaminar flow-based PE deposition onto the magnetic droplets (100 ± 0.5 μm diameter), attempts were made to deflect them through fluorescently labelled, cationic poly(allylamine hydrochloride) (PAH-FITC). The droplets were deflected freely through the washing solutions, when they reached the PAH-FITC interface the oil-based ferrofluid drops instantly stuck to the surface of the chip, agglomerating together throughout the affected region of the chamber and ensuring that no stable droplets survived the procedure (ESI Fig. S5). This may have occurred due to several possible reasons. Firstly, the droplets, which were effectively "squashed" in the shallow chamber, were susceptible to wall effects that could have stripped the SDS surfactant monolayer from the droplet surfaces. Secondly, SDS is a small-molecule anionic surfactant which is in a dynamic equilibrium of adsorption and desorption at an oil-water (O/W) interface. Consequently, when droplets were deflected from the SDS continuous phase stream into the Tween20 and PE streams, the droplets surface would be not-fully coated by the surfactant and would become prone to coalescence with earlier formed drops.

In order to overcome these challenges, the wall effects caused by the shallow chip designs were eliminated by employing a "deeper" channel design. The goal here was to generate small droplets in a shallow droplet generation channel before they entered a deep reaction chamber, whereupon they would take on a spherical shape that was too small to contact the chamber surfaces. Furthermore, a polymeric surfactant, poly(vinyl pyrrolidone) (PVP) was employed instead of SDS to provide better droplet stability.

Magnetic droplet manipulation in the deep chip design

The deep chip designs were prepared by etching two glass plates: the top plate featuring a shallow droplet generation junction (20 μm deep) and the bottom plate having a deep reaction chamber (100 μm height). As in the previous studies with the shallow chip design, initial tests involved the study of the effect of the DP and CP flow rates on droplet sizes in a flow-focusing design (DGF4) and T-junction designs (DGT5 and DTG6). The results are shown in ESI Fig. S7. In each case, droplets were generated in the shallow part of the chip, having a flattened disc shape, but then adopted a spherical shape when they entered the deeper region of the chip. This process can be observed in "**ESI Video 2 - Droplet generation in deep chip design DGF4.mp4**".

The flow-focusing DGF4 design was then used for magnetic droplet deflection studies, in which the droplet trajectories were investigated using different sizes and types (NdFeB or SmCo) of magnets. These were also placed at varying distances from the deflection chamber, thus providing a range of magnetic flux densities (**B**) and gradients (∇**B**) experienced by the droplets in the chamber (see ESI Section 2.3, including Figs. S8 and S9). The optimum magnetic setup involved the use of a 3.0 x 4.8 x 7.3 mm^3 SmCo magnet placed 8.5 mm from the chamber, allowing the droplets to be deflected to outlet 5 with a shallow trajectory. Further tests were performed to determine the effect of dilution of the ferrofluid on the deflection trajectories. The findings showed that a 1:1 dilution of the ferrofluid with cyclohexane (yielding 1.12 x 10^6 magnetic nanoparticles pL^{-1}) before its introduction into the chip yielded optimum performance (ESI Fig. S10 and Table S3).

The deflection of magnetic droplets through multilaminar reagent streams was performed much in the same way as for the shallow chip design. In the first tests, magnetic droplets were successfully deflected through alternating streams of red and blue inks, and demonstrated minimal disturbance of the interface as they passed from one stream to the next (ESI Fig. S11). The deflection of magnetic droplets through streams of ink can be observed in "**ESI Video 3 - Droplet deflection in deep chip design.mp4**", though it should be noted that this video was taken using a black and white CCD camera.

In the following test, the deposition of a single PE layer onto droplets was investigated via their deflection through a stream of fluorescently labelled anionic poly(acrylic acid) (PAA-Rhod123) (Fig. 4a). In the deep channel chamber, where the droplets were spherical rather being pressed between the top and bottom of the chip as had been the case in the shallow chip design, the PVP-stabilised magnetic droplets were deflected across the chamber, passing through the PAA-Rhod123 stream before being washed in the next stream and then exiting the chamber via outlet 5. The collected droplets showed a high degree of monodispersity (68.9 ± 1.8 μm) and stability (Fig. 4b). The droplets, which are not usually fluorescent, also exhibited a fluorescence signal that indicated deposition of the PAA-Rhod123 onto the droplets (Figs. 4c,d). Thus, magnetic droplet templates were successfully generated and coated with a layer of fluorescently tagged PE, with a subsequent washing step, within 10 – 15 seconds; a significant improvement in processing times.

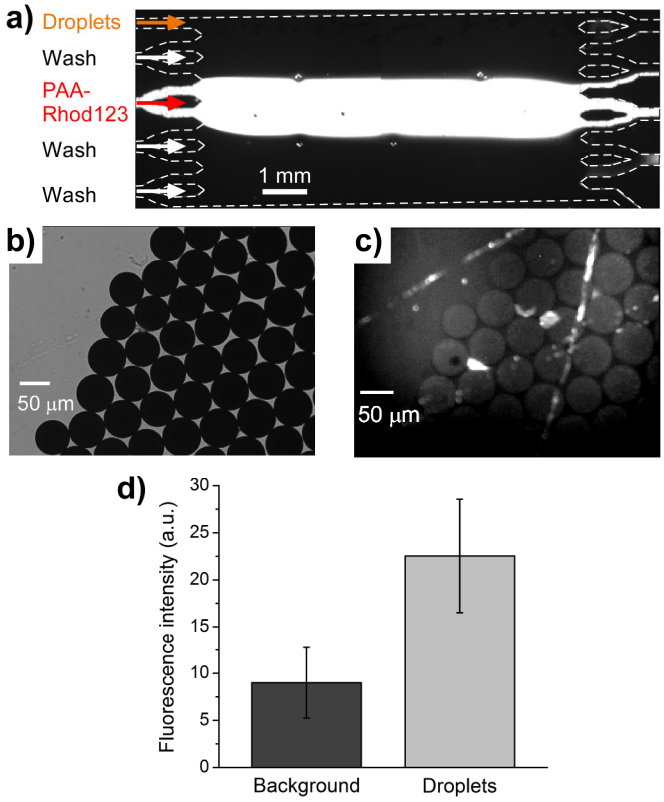

Fig. 4 Deflection of PVP-stabilised magnetic droplets through a polyelectrolyte stream of Rhodamine 123-labeled poly(acrylic acid) (PAA-Rhod123) and into a washing stream via an SmCo magnet in the "deep" DGF4 chip design. (a) Photograph of the deep DGF4 reaction chamber with the PAA-Rhod123. (b) PAA-Rhod123 coated magnetic droplets collected from outlet 5. (c) Fluorescence image of the collected droplets. (d) Fluorescence intensities of the collected droplets, demonstrating successful coating with fluorescently tagged PAA-Rhod123.

However, the deposition of multiple PE layers onto magnetic droplets was often experimentally challenging using the deep chip design. The co-flowing streams of PE and washing solutions in the chamber were easily influenced by slight disturbances, such as when the tubing was accidentally knocked or the chip moved on the microscope stage for observation. In this scenario, the PE solution streams and/or magnetic droplets could exit via the wrong outlets, leading us to propose a new chip design that could overcome these issues and provide a stable guide for the streams, resulting in a more robust platform.

Magnetic droplet manipulation in the "Snakes-and-Ladders" chip

The lessons learned from the shallow and deep chip designs led to the development of a chip design akin to the "Snakes-and-Ladders" boardgame, in which the laminar reagent streams were separated into 5 parallel channels rather than flowing into a single chamber (Fig. 2e,f). These main channels were interconnected via small side channels that allowed the deflection of magnetic droplets from one channel to the next. This restricted the trajectories of the magnetic droplets and ensured greater reproducibility. As in previous examples, droplet generation and magnetic deflection were studied before attempting the deflection of magnetic droplets through PE streams.

Droplet generation. The "Snakes-and-Ladders" chip used here featured a flow-focusing droplet generation junction (Fig. 2e,f), the same as that used for the deep channel chip due to the interchangeable nature of the designs, and this was aligned and bonded to the deeper droplet inlet channel of the "Snakes-and-Ladders" structure. Oil-based ferrofluid DP was pumped into the inlet 1 at a flow rate of 1 μL h^{-1} while a CP of aqueous PVP solution (10 mg mL^{-1}) was pumped into inlet 2 at a range of flow rates between 100 and 500 μL h^{-1} to determine the effect on droplet size. As in the deep chip, the generated droplets were squashed into disc shapes in the shallow flow-focusing channel, before entering the deeper channel where they took on a spherical shape (Fig. 5a). At the range of flow rates employed, spherical magnetic droplets were generated with diameters of 37 - 59 μm (Fig. 5b).

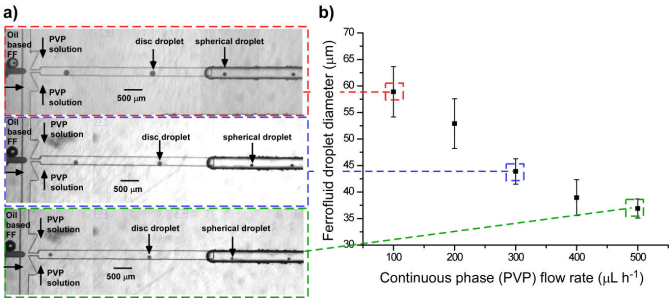

Fig. 5 Photographs of oil-based ferrofluid droplets generated in the "Snakes-and-Ladders" chip at a flow-focusing junction. Droplets generated in the 20 μm deep channel in the top layer of the chip were initially disc shaped, but became spherical upon entering the 100 μm deep bottom layer. The photographs show droplets generated at a ferrofluid flow rate of 1 μL h^{-1} and aqueous PVP flow rates of: 100 μL h^{-1} (upper image), 300 μL h^{-1} (middle image), and 500 μL h^{-1} (lower image). (b) Droplet diameter (measured in the deep section of the chip) as a function of PVP continuous phase flow rate at a ferrofluid flow rate of 1 μL h^{-1}.

Droplet deflection studies. PVP-stabilised magnetic droplets of 43 ± 2 μm diameter were generated based on flow rates determined in the previous section, and introduced into the "Snakes-and-Ladders" chip structure. Alternating streams of red and blue inks were pumped into the chip in order to visualise the streams in the channel structure and to observe the passage of magnetic droplets through the streams. The deflection of droplets was studied by placing the SmCo magnet (3 x 4.8 x 7.3 mm^3), as used previously, at varying distances from the lower edge of channel 5 and at different flow rates.

In the first instance, the magnet was placed 7.5 mm from channel 5 and flow rates of either 300 μL h^{-1} (linear velocity of 2.08 mm s^{-1}) or 500 μL h^{-1} (linear velocity of 3.47 mm s^{-1}) were

applied. In the presence of the external magnet, the droplets moved along the each channel until they reached an interconnect channel, where they were deflected through the interconnected channel into the next parallel channel, with the process repeating at each interconnect. At a flow rate 300 μL h^{-1}, the droplets were deflected through the entire chip, passing through each ink stream and into channel 5 (ESI Fig. S12). At 500 μL h^{-1}, however, the droplets were only deflected as far as channel 3 and thus unable to cross each stream.

As part of the same set of tests, the distance of the magnet from channel 5 was also varied between 7.5 mm and 10.5 mm while a flow rate of 300 μL h^{-1}. This demonstrated how the location of the magnet was crucial, as moving it only 3 mm further from the channel to a distance of 10.5 mm resulted in the droplets only deflecting as far as channel 2 (ESI Fig. S13). A video of droplet deflection through ink streams in the "Snakes-and-Ladders" chip design can be seen in "**ESI Video 4 - Droplet deflection in Snakes-and-Ladders chip design.mp4**".

Droplet deflection through PE streams. With optimum deflection conditions determined via the previous tests, the ability to deposit two layers of PE onto the magnetic droplets was investigated using the "Snakes-and-Ladders" chip. PVP-stabilised magnetic droplets (43 ± 2 μm diameter) were and deflected through the channel structure via the SmCo magnet, which was placed 7.5 mm from channel 5. Negatively charged PSS (10 mg mL^{-1}) polyelectrolyte was pumped into inlet 3, while positively charged fluorescent PAH-FITC (1 mg mL^{-1}, with 0.05 % v/v Tween60) was pumped into inlet 6, and washing solutions composed of pure water was pumped into inlets 4 and 5 (Fig. 6a).

A computational analysis of the magnetic flux density (**B**) and magnetic force on the droplets ($\mathbf{F_{mag}}$) across the channels of the "Snakes-and-Ladders" chip was performed,[70, 71] and the results are shown in Fig. 6b. The $\mathbf{F_{mag}}$ forces on the droplets were estimated to increase from 0.1 to 1 nN as they passed through the chip due to the increase in **B** from about 8 to 23 mT. This force field was sufficient to deflect the droplets through each of the channels without causing any aggregation, which would have yielded a lower encapsulation efficiency. As such, the droplet passed sequentially through the streams of PSS solutions, washing solution, and PAH-FITC solution (Fig. 6c), before being collected for analysis via fluorescence microscopy as shown in Fig. 6.

Due to the lack of a final washing stream in this particular experimental setup, the droplets were collected in the PAH-FITC solution that was in channel 5, i.e. the final channel of the device. As a result, the background in Fig. 7a has a high fluorescence intensity, but the droplets can be clearly be distinguished against the background, indicating successful deposition of the PAH-FITC onto the droplet surfaces. This is not ideal, however, and would be addressed in future iterations of the device via the addition of a washing stream in the final channel, regardless of how many PE reagent streams were present in the device.

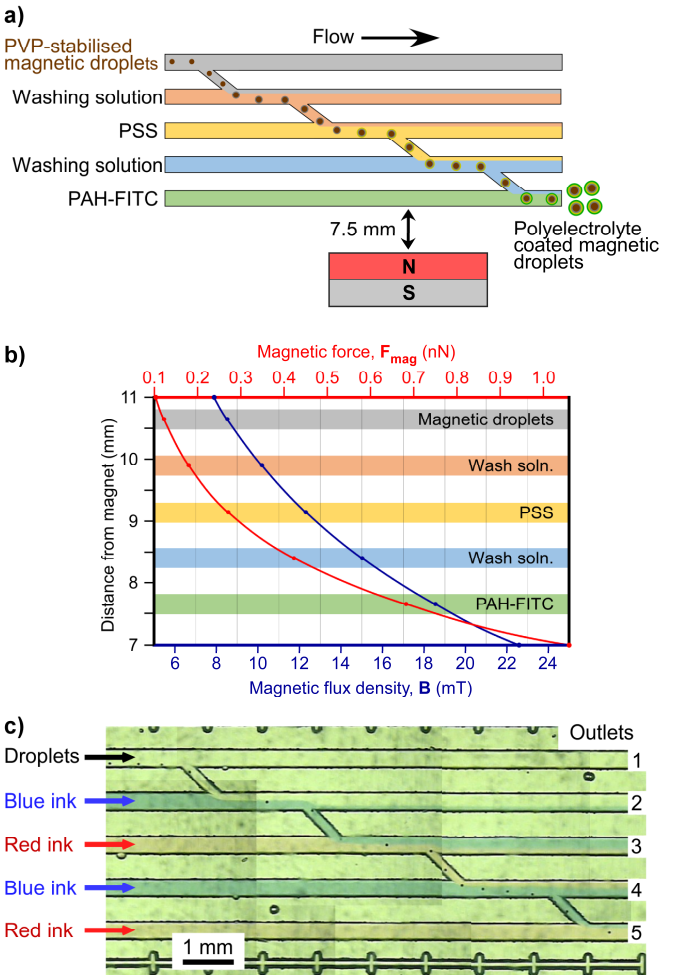

Fig. 6 (a) Principle of the deflection of magnetic droplets through multiple reagent and washing streams using the Snakes-and-Ladders chip. An SmCo was placed 7.5 mm from the edge of the lowest channel. The example shows the setup for the deposition of PE layers on the PVP-stabilised magnetic droplets via their deflection through the anionic PSS and the cationic, fluorescent PAH-FITC streams. (b) Magnetic flux density (**B**) across the chip and the magnetic forces acting on the droplets ($\mathbf{F_{mag}}$). (c) Photograph showing the deflection of magnetic droplets through multiple alternating ink streams for visualisation of the streams. The image was constructed from multiple photographs of different regions of the chip.

Furthermore, although only the final PE stream, composed of positively charged PAH-FITC, was fluorescently labelled, the fact that the droplets were fluorescent after passing through each stream implies the successful coating of PSS onto the droplets. The direct observation of PSS coating could not be obtained due to the lack of a fluorescent dye on that PE, since unlike PAH-FITC there is no commercially available fluorescent option for PSS. However, the indirect observation of deposition was achieved as the PAH-FITC could only be adsorbed onto the droplets in the presence of PSS. In other words, if the negatively-charged PSS was not present, the positively-charged PAH-FITC would not be able to adsorb to the positively-charged PAA-stabilised droplets.

The deposition of a PE bilayer occurred in <10 s, with <30 s required in total for droplet generation, PE coating, and washing. This demonstrates the potential of this platform for

the rapid preparation of multi-layered PE capsules (PMLCs) in an automated fashion. While droplets were used as the templates here, this "Snakes-and-Ladders" chip design could also be applied solid templates, e.g. solid microparticles and cells. The "Snakes-and-Ladders" chip design improved flow stability but also enhanced the efficiency of droplet deflection and collection through the desired outlet by constraining the trajectory of the magnetic droplets.

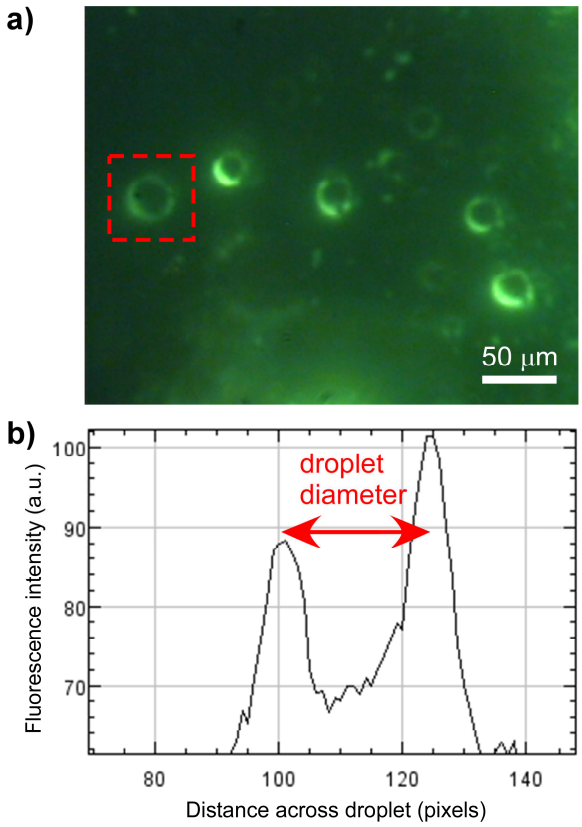

Fig 7 Magnetic droplets collected from the "Snakes-and-Ladders" chip after passing through streams of PSS and fluorescent PAH-FITC. (a) Fluorescence microscope image of the collected droplets. (b) Fluorescence intensity of a representative magnetic droplet, demonstrating an increase in fluorescence intensity compared to the background that indicates a successful coating with PSS and PAH-FITC.

In addition, the residence time of the droplets in the reagent streams could be tuned simply by the hydrodynamic flow velocity ($\mathbf{u_{hyd}}$), controlled by the applied flow rates, and the magnetic-induced velocity ($\mathbf{u_{mag}}$), controlled by the magnet size, type and location, in addition to the channel lengths. Additional PE coatings could be added to the droplets by increasing the number of PE solutions and washing channels, or by adding interconnecting channels to allow the magnetic droplets to move back-and-forth through the PE and washing streams in a zig-zag motion via multiple magnets, a technique employed previously for bioassays on magnetic particles.[73, 74]

Conclusions

We have presented microfluidic devices for the generation of oil-based ferrofluid droplets in an aqueous continuous phase, and their downstream magnetic deflection across parallel streams for the continuous layer-by-layer (LbL) coating of the droplet templates with polyelectrolyte (PE). The use of a chip design akin to the "Snakes-and-Ladders" board game enabled stable flow streams and controlled droplet trajectories, achieving PE bilayer deposition and washing in <30 s. This represented a significant reduction in processing times compared to conventional LbL deposition that are rendered time-consuming due to the consecutive reaction and multiple washing steps required. It should be relatively straightforward to include additional PE and washing streams that would allow the LbL deposition of multiple PE layers onto the magnetic droplets, towards the fabrication of multilayered PE capsules (PMLCs) for potential drug delivery applications.

Furthermore, the two-layered "Snakes-and-Ladders" chip represented the culmination of improvements developed to solve a number of issues that had been encountered when using shallow chips and designs with wide reaction chambers, and could easily be adapted to the coating of solid templates, or for performing a number of other applications, e.g. magnetic particle-based assays.

Acknowledgements

The authors thank the Royal Embassy of Saudi Arabia Cultural Bureau in London and Albaha University in Saudi Arabia for funding. J.G.-P., E.B. and I.O. acknowledge financial support from the Spanish Ministry of Economy and Competitiveness (project CTQ2015-66078-R (MINECO/FEDER) and FPI postgraduate research grant (BES-2013-064415). The authors thank Dr Stephen Clark for fabrication of the microfluidic devices.

References

1. M. M. de Villiers and Y. M. Lvov, *Adv. Drug Deliv. Rev.*, 2011, **63**, 699-700.
2. S. De Koker, R. Hoogenboom and B. G. De Geest, *Chem. Soc. Rev.*, 2012, **41**, 2867-2884.
3. W. Tong, X. Song and C. Gao, *Chem. Soc. Rev.*, 2012, **41**, 6103-6124.
4. M. McShane and D. Ritter, *J. Mater. Chem.*, 2010, **20**, 8189-8193.
5. P. Rivera_Gil, M. Nazarenus, S. Ashraf and W. J. Parak, *Small*, 2012, **8**, 943-948.
6. E. W. Stein, D. V. Volodkin, M. J. McShane and G. B. Sukhorukov, *Biomacromolecules*, 2006, **7**, 710-719.
7. W. Qi, L. Duan and J. Li, *Soft Matter*, 2011, **7**, 1571-1576.
8. F. Caruso, R. A. Caruso and H. Mohwald, *Science*, 1998, **282**, 1111-1114.
9. G. Decher, *Science*, 1997, **277**, 1232-1237.
10. Y. Yan, M. Björnmalm and F. Caruso, *Chem. Mater.*, 2014, **26**, 452-460.

11. R. F. Fakhrullin, J. Garcia-Alonso and V. N. Paunov, *Soft Matter*, 2010, **6**, 391-397.
12. R. F. Fakhrullin, A. I. Zamaleeva, R. T. Minullina, S. A. Konnova and V. N. Paunov, *Chem. Soc. Rev.*, 2012, **41**, 4189-4206.
13. D. J. McClements, *Curr. Opin. Colloid Interface Sci.*, 2012, **17**, 235-245.
14. E. M. Shchukina and D. G. Shchukin, *Curr. Opin. Colloid Interface Sci.*, 2012, **17**, 281-289.
15. B. G. De Geest, N. N. Sanders, G. B. Sukhorukov, J. Demeester and S. C. De Smedt, *Chem. Soc. Rev.*, 2007, **36**, 636-649.
16. H. Ai, S. A. Jones, M. M. de Villiers and Y. M. Lvov, *J. Control. Release*, 2003, **86**, 59-68.
17. L. Dahne, S. Leporatti, E. Donath and H. Mohwald, *J. Am. Chem. Soc.*, 2001, **123**, 5431-5436.
18. A. Voigt, H. Lichtenfeld, G. B. Sukhorukov, H. Zastrow, E. Donath, H. Baumler and H. Mohwald, *Ind. Eng. Chem. Res.*, 1999, **38**, 4037-4043.
19. M. D. Tarn and N. Pamme, Microfluidics, in *Elsevier Reference Module in Chemistry, Molecular Sciences and Chemical Engineering*, ed. J. Reedijk, Elsevier, Waltham, MA, 2013.
20. S. Minnikanti, A. Gangopadhyay and D. Reyes, *Polymers*, 2014, **6**, 2100.
21. J. J. Richardson, J. Cui, M. Björnmalm, J. A. Braunger, H. Ejima and F. Caruso, *Chem. Rev.*, 2016, **116**, 14828-14867.
22. D. Liu, H. Zhang, F. Fontana, J. T. Hirvonen and H. A. Santos, *Lab Chip*, 2017, doi: 10.1039/c1037lc00242d.
23. G. Kaufman, R. Boltyanskiy, S. Nejati, A. R. Thiam, M. Loewenberg, E. R. Dufresne and C. O. Osuji, *Lab Chip*, 2014, **14**, 3494-3497.
24. G. Kaufman, S. Nejati, R. Sarfati, R. Boltyanskiy, M. Loewenberg, E. R. Dufresne and C. O. Osuji, *Soft Matter*, 2015, **11**, 7478-7482.
25. L. Zhang, L.-H. Cai, P. S. Lienemann, T. Rossow, I. Polenz, Q. Vallmajo-Martin, M. Ehrbar, H. Na, D. J. Mooney and D. A. Weitz, *Angew. Chem. Int. Ed.*, 2016, **55**, 13470-13474.
26. M. D. Tarn, M. J. Lopez-Martinez and N. Pamme, *Anal. Bioanal. Chem.*, 2014, **406**, 139-161.
27. C. Priest, A. Quinn, A. Postma, A. N. Zelikin, J. Ralston and F. Caruso, *Lab Chip*, 2008, **8**, 2182-2187.
28. C. Kantak, S. Beyer, L. Yobas, T. Bansal and D. Trau, *Lab Chip*, 2011, **11**, 1030-1035.
29. B. Ayan, A. Ozcelik, H. Bachman, S.-Y. Tang, Y. Xie, M. Wu, P. Li and T. J. Huang, *Lab Chip*, 2016, **16**, 4366-4372.
30. N. Pamme, *Lab Chip*, 2006, **6**, 24-38.
31. N. Pamme, *Curr. Opin. Chem. Biol.*, 2012, **16**, 436-443.
32. M. A. M. Gijs, *Microfluid. Nanofluid.*, 2004, **1**, 22-40.
33. M. A. M. Gijs, F. Lacharme and U. Lehmann, *Chem. Rev.*, 2010, **110**, 1518-1563.
34. S. S. H. Tsai, J. S. Wexler, J. Wan and H. A. Stone, *Appl. Phys. Lett.*, 2011, **99**, 153509.
35. S. G. Jones, N. Abbasi, B.-U. Moon and S. S. H. Tsai, *Soft Matter*, 2016, **12**, 2668-2675.
36. B.-U. Moon, N. Hakimi, D. K. Hwang and S. S. H. Tsai, *Biomicrofluidics*, 2014, **8**, 052103.
37. S. A. Peyman, A. Iles and N. Pamme, *Chem. Commun.*, 2008, 1220-1222.
38. S. A. Peyman, A. Iles and N. Pamme, *Lab Chip*, 2009, **9**, 3110-3117.
39. S. A. Peyman, H. Patel, N. Belli, A. Iles and N. Pamme, *Magnetohydrodynamics*, 2009, **45**, 361-370.
40. C. Phurimsak, M. D. Tarn, S. A. Peyman, J. Greenman and N. Pamme, *Anal. Chem.*, 2014, **86**, 10552-10559.
41. M. D. Tarn, L. T. Elders, S. A. Peyman and N. Pamme, *RSC Adv.*, 2015, **5**, 103776-103781.
42. M. Vojtisek, A. Iles and N. Pamme, *Biosens. Bioelectron.*, 2010, **25**, 2172-2176.
43. M. D. Tarn, R. F. Fakhrullin, V. N. Paunov and N. Pamme, *Mater. Lett.*, 2013, **95**, 182-185.
44. I. Torres-Diaz and C. Rinaldi, *Soft Matter*, 2014, **10**, 8584-8602.
45. N.-T. Nguyen, *Microfluid. Nanofluid.*, 2012, **12**, 1-16.
46. W. Zhao, R. Cheng, J. R. Miller and L. Mao, *Adv. Funct. Mater.*, 2016, **26**, 3916-3932.
47. Z. Z. Chong, S. H. Tan, A. M. Ganan-Calvo, S. B. Tor, N. H. Loh and N.-T. Nguyen, *Lab Chip*, 2016, **16**, 35-58.
48. H. Song, D. L. Chen and R. F. Ismagilov, *Angew. Chem. Int. Ed.*, 2006, **45**, 7336-7356.
49. S.-Y. Teh, R. Lin, L.-H. Hung and A. P. Lee, *Lab Chip*, 2008, **8**, 198-220.
50. P. Zhu and L. Wang, *Lab Chip*, 2017, **17**, 34-75.
51. S. Afkhami, A. J. Tyler, Y. Renardy, M. Renardy, T. G. St. Pierre, R. C. Woodward and J. S. Riffle, *J. Fluid Mech.*, 2010, **663**, 358-384.
52. T. Say-Hwa, N. Nam-Trung, Y. Levent and K. Tae Goo, *J. Micromech. Microeng.*, 2010, **20**, 045004.
53. E. Al-Hetlani, O. J. Hatt, M. Vojtisek, M. D. Tarn, A. Iles and N. Pamme, *AIP Conf. Proc.*, 2010, **1311**, 167-175.
54. K. Zhang, Q. Liang, S. Ma, X. Mu, P. Hu, Y. Wang and G. Luo, *Lab Chip*, 2009, **9**, 2992-2999.
55. A. Beyzavi and N.-T. Nguyen, *J. Micromech. Microeng.*, 2010, **20**, 015018.
56. Y. Wu, T. Fu, Y. Ma and H. Z. Li, *Soft Matter*, 2013, **9**, 9792-9798.
57. Y. Wu, T. Fu, Y. Ma and H. Z. Li, *Microfluid. Nanofluid.*, 2015, **18**, 19-27.
58. S. Kahkeshani and D. Di Carlo, *Lab Chip*, 2016, **16**, 2474-2480.
59. V. B. Varma, A. Ray, Z. Wang, R. Wu, P. J. Jayaneel, N. M. Sudharsan and R. V. Ramanujan, *IEEE Magn. Lett.*, 2016, **7**, 1-5.
60. V. B. Varma, A. Ray, Z. M. Wang, Z. P. Wang and R. V. Ramanujan, *Sci. Rep.*, 2016, **6**.
61. A. Ray, V. B. Varma, P. J. Jayaneel, N. M. Sudharsan, Z. P. Wang and R. V. Ramanujan, *Sens. Actuators B Chem.*, 2017, **242**, 760-768.
62. Y. Jo, F. Shen, Y. K. Hahn, J. H. Park and J. K. Park, *Micromachines*, 2016, **7**.
63. K. Zhang, Q. Liang, X. Ai, P. Hu, Y. Wang and G. Luo, *Lab Chip*, 2011, **11**, 1271-1275.
64. K. Zhang, Q. Liang, X. Ai, P. Hu, Y. Wang and G. Luo, *Anal. Chem.*, 2011, **83**, 8029-8034.
65. N. Pamme and A. Manz, *Anal. Chem.*, 2004, **76**, 7250-7256.
66. M. D. Tarn, S. A. Peyman, D. Robert, A. Iles, C. Wilhelm and N. Pamme, *J. Magn. Magn. Mater.*, 2009, **321**, 4115-4122.
67. N. Pamme and C. Wilhelm, *Lab Chip*, 2006, **6**, 974-980.
68. A. Laguecir, S. Ulrich, J. Labille, N. Fatin-Rouge, S. Stoll and J. Buffle, *Eur. Polym. J.*, 2006, **42**, 1135-1144.
69. T. McCreedy, *TrAC Trends Anal. Chem.*, 2000, **19**, 396-401.
70. J. Gómez-Pastora, I. H. Karampelas, X. Xue, E. Bringas, E. P. Furlani and I. Ortiz, *J. Phys. Chem. C*, 2017, **121**, 7466-7477.
71. J. Gómez-Pastora, X. Xue, I. H. Karampelas, E. Bringas, E. P. Furlani and I. Ortiz, *Sep. Purif. Technol.*, 2017, **172**, 16-31.
72. E. P. Furlani, *Permanent Magnet and Electromechanical Devices; Materials, Analysis and Applications*, Academic Press, New York, 2001.

73. L. A. Sasso, A. Ündar and J. D. Zahn, *Microfluid. Nanofluid.*, 2010, **9**, 253-265.
74. Y. Gao, A. W. Y. Lam and W. C. W. Chan, *ACS Appl. Mater. Interfaces*, 2013, **5**, 2853-2860.

